Check for updates

Received: 22 February 2023 | Revised: 14 June 2023 | Accepted: 18 June 2023

DOI: 10.1002/bit.28484

ARTICLE

BIOTECHNOLOGY AND BIOENGINEERING WILEY

Engineering and characterization of carbohydrate-binding modules for imaging cellulose fibrils biosynthesis in plant protoplasts

Dharanidaran Jayachandran[1] | Peter Smith[2] | Mohammad Irfan[1] | Junhong Sun[3] | John M. Yarborough[2] | Yannick J. Bomble[2] | Eric Lam[3] | Shishir P. S. Chundawat[1]

[1]Department of Chemical and Biochemical Engineering, Rutgers-The State University of New Jersey, Piscataway, New Jersey, USA

[2]National Renewable Energy Laboratory, Biosciences Center, Golden, Colorado, USA

[3]Department of Plant Biology, Rutgers-The State University of New Jersey, New Brunswick, New Jersey, USA

Correspondence

Shishir P. S. Chundawat, Department of Chemical and Biochemical Engineering, Rutgers-The State University of New Jersey, Piscataway, NJ 08854, USA.
Email: shishir.chundawat@rutgers.edu

Funding information

US Department of Energy; Center for Bioenergy Innovation

Abstract

Carbohydrate binding modules (CBMs) are noncatalytic domains that assist tethered catalytic domains in substrate targeting. CBMs have therefore been used to visualize distinct polysaccharides present in the cell wall of plant cells and tissues. However, most previous studies provide a qualitative analysis of CBM-polysaccharide interactions, with limited characterization of engineered tandem CBM designs for recognizing polysaccharides like cellulose and limited application of CBM-based probes to visualize cellulose fibrils synthesis in model plant protoplasts with regenerating cell walls. Here, we examine the dynamic interactions of engineered type-A CBMs from families 3a and 64 with crystalline cellulose-I and phosphoric acid swollen cellulose. We generated tandem CBM designs to determine various characteristic properties including binding reversibility toward cellulose-I using equilibrium binding assays. To compute the adsorption (nk_{on}) and desorption (k_{off}) rate constants of single versus tandem CBM designs toward nanocrystalline cellulose, we employed dynamic kinetic binding assays using quartz crystal microbalance with dissipation. Our results indicate that tandem CBM3a exhibited the highest adsorption rate to cellulose and displayed reversible binding to both crystalline/amorphous cellulose, unlike other CBM designs, making tandem CBM3a better suited for live plant cell wall biosynthesis imaging applications. We used several engineered CBMs to visualize *Arabidopsis thaliana* protoplasts with regenerated cell walls using confocal laser scanning microscopy and wide-field fluorescence microscopy. Lastly, we also demonstrated how CBMs as probe reagents can enable in situ visualization of cellulose fibrils during cell wall regeneration in Arabidopsis protoplasts.

KEYWORDS

Arabidopsis plant protoplasts, carbohydrate-binding module, cell wall biosynthesis, cellulose microfibrils, live-cell imaging, quartz crystal microbalance with dissipation

This is an open access article under the terms of the Creative Commons Attribution-NonCommercial-NoDerivs License, which permits use and distribution in any medium, provided the original work is properly cited, the use is non-commercial and no modifications or adaptations are made.
© 2023 The Authors. *Biotechnology and Bioengineering* published by Wiley Periodicals LLC.

1 | INTRODUCTION

Plant cell walls are structurally complex, metabolically dynamic, and extremely rich polysaccharide repositories. Cell wall polysaccharides mainly comprise of cellulose, hemicelluloses, and pectin, that form complex polymer networks that are extensively connected with each other (Knox, 2008). Cellulose microfibrils form the major component of the plant cell wall and are intertwined with xyloglucans and other pectic polysaccharides. To target different polysaccharides, plant cell wall hydrolase enzymes have evolved highly specific, noncatalytic carbohydrate-binding modules (CBMs) along with catalytic domains (CD). These CBMs increase the proximity between CDs and polysaccharides, resulting in efficient enzymatic hydrolysis (Talamantes et al., 2016). Different CBMs recognize different polysaccharides based on their amino acid sequences and the topology of the binding site. According to the Carbohydrate-Active enZYmes (CAZy) database (http://www.cazy.org), there are 94 sequence-based families of CBMs, many of which bind to cell wall polymers (Drula et al., 2022). For instance, type-A CBM recognizes crystalline polysaccharides such as cellulose, chitin, and mannan. Likewise, type-B CBMs target individual glucan chains, and type-C CBMs bind specifically to small sugars (mono- or disaccharides) (Boraston et al., 2004). Most CBMs are highly specific, and their specificity depends on the target substrate of its accompanying CD. However, some cellulose-binding CBMs have been reported to be components of multifunctional enzymes that also hydrolyze xylans, mannans, and pectins (Kellett et al., 1990; McKie et al., 2001).

In nature, noncatalytic CBMs are sometimes found to coexist with other noncatalytic CBMs besides CDs, forming tandem repeats of CBMs. Such tandem CBMs increase the cell wall hydrolases' overall efficiency by enhancing affinity through prolonged contact with the target substrate (Guillén et al., 2010; Hashimoto, 2006; Møller et al., 2021). For example, a type-A tandem CBM with three CBM10 domains associated with mannanase showed improved binding and spatial flexibility (Møller et al., 2021). Similarly, type-B CBM tandems (CBM17 and CBM28) from *Bacillus* sp. 1139 Cel5 and two family 4 CBMs (CBM4–1 and CBM4–2) from *Cellulomonas* sp. exhibited very tight noncrystalline cellulose binding. Taken individually, these three CBMs recognized different regions of noncrystalline cellulose (Boraston et al., 2003; Kognole & Payne, 2018). Aside from hydrolysis of celluloses, only a few of these tandem CBMs have been engineered to visualize polysaccharides associated with plant cell walls. For example, Herve et al. (2010) found that the CBM3a·CBM2b-1-2 tandem constructs bound tightly to cell wall of stem sections where cellulose and xylan were cross-linked closely. But no reports indicate the use of tandem CBMs in imaging cell walls in single plant protoplasts yet. Living plant protoplasts provide a distinct advantage as a cell-based system that can be readily used for performing genomics, transcriptomics, proteomics, metabolomics, and epigenetic analyses (Xu et al., 2022). This versatile system could be used to characterize the cell-wall biosynthesis process and the polysaccharides associated with the regenerated protoplast cell walls. Additionally, regenerating protoplast plant cell walls in *Arabidopsis* contain both crystalline and amorphous regions at the surface (Ruel et al., 2012). It is thus imperative that the CBMs' ability to bind to various forms of cellulose is characterized critically before implementation as visualization probes.

Extensive research has been conducted on CBMs attached to hydrolases using bulk biochemical assays (Chundawat et al., 2021; Nemmaru et al., 2021), single-molecule cellulase motility assays (Brady et al., 2015), kinetic modeling (Levine et al., 2010; Shang et al., 2013), and molecular simulations (Beckham et al., 2014; Vermaas et al., 2019). However, most of these assays have been conducted on single CBMs attached to either fluorescent proteins or hydrolases. Consequently, the biochemical behavior of most tandem CBMs under the assays mentioned above has not been extensively studied despite the prevalence of tandem CBMs designs in natural systems (Boraston et al., 2004; Hervé et al., 2010; McCartney et al., 2006). Ultimately, the potential of tandem CBMs in the visualization and characterization of cell wall polymers remains mostly unexplored.

Here, using engineered CBM constructs, we determined the different binding parameters for several tandem versus single CBM designs. We picked two model type-A CBMs (namely CBM3a and CBM64) and systematically engineered several tandem versions with and without green fluorescent protein (GFP). Using conventional pull-down assays, we calculated the number of binding sites, binding constants, and partition coefficient toward cellulose-I and phosphoric acid swollen cellulose (PASC) as model substrates. Using quartz crystal microbalance with dissipation (QCM-D), we next measured the adsorption and desorption rate constants (nk_{on} and k_{off}) for engineered CBM binding toward nanocrystalline cellulose-I. Finally, we used the CBMs generated to visualize the regenerated cell walls in *Arabidopsis thaliana* plant protoplasts to demonstrate their potential in visualization of plant cell wall polysaccharides like cellulose using confocal laser scanning microscopy (CLSM) and wide-field fluorescence microscopy.

2 | MATERIALS AND METHODS

2.1 | Bacterial strains, CBM plasmids, and reagents

Avicel cellulose-I was obtained from Sigma Aldrich under the label Avicel PH-101. Phusion Master Mix was obtained from Thermo Fisher Scientific. Dpn1 and T4 DNA polymerase was obtained from New England Biolabs. Nickel-charged magnetic beads and magnetic racks were purchased from GenScript. Chemically competent cells were procured from various vendors: *E. cloni* 10G cells from Lucigen and *E. coli* BL21-CodonPlus-RIPL [λDE3] from Stratagene. The pEC-GFP-CBM3a vector was kindly provided by Dr. Brian Fox (University of Wisconsin) and was used as plasmid backbone to engineer all CBM constructs as done previously (Chundawat et al., 2021; Whitehead et al., 2017). The primers were obtained from Integrated DNA technologies, and DNA sequencing was performed by Azenta Life Sciences. All other reagents were

10970290, 2023, 8, Downloaded from https://onlinelibrary.wiley.com/doi/10.1002/bit.28484 by National Renewable Energy Lab, Wiley Online Library on [03/08/2023]. See the Terms and Conditions (https://onlinelibrary.wiley.com/terms-and-conditions) on Wiley Online Library for rules of use; OA articles are governed by the applicable Creative Commons License

purchased from VWR, Thermo Fisher Scientific, and Sigma Aldrich unless mentioned otherwise.

2.2 | Synthesis and cloning of wild-type CBM genes into pEC-GFP vector

E. coli expression vector pEC-GFP-CBM3a and pEC-DSR-CBM3a was kindly provided by the Fox lab (UW Madison) (Whitehead et al., 2017), which was used as the plasmid backbone to insert the CBM64 gene from *Spirochaeta thermophila*. GFP and DSR are green fluorescent protein and discosoma red protein, respectively. Cloning and insertion of CBM64 are detailed in our previous work (Nemmaru et al., 2021). Plasmid maps for pEC-GFP-CBM3a and pEC-GFP-CBM64 are outlined in Supporting Information: Figure S1. Tandem CBMs (pEC-GFP-CBM3a-CBM3a, pEC-CBM3a-CBM3a, pEC-GFP-CBM64-CBM64, and pEC-CBM64-CBM64) were prepared from the original plasmids (pEC-GFP-CBM3a and pEC-GFP-CBM64) using Sequence and Ligation-Independent Cloning (SLIC) protocol (Stevenson et al., 2013). Similarly, CBM17 gene from *Clostridium cellulovarans* was also used to generate pEC-GFP-CBM17, pEC-CBM17, and pEC-CBM17-CBM17 constructs. All the CBM constructs had a 42 amino acid native linker between GFP and CBM as well as between the tandem CBM residues. The schematic representation of all CBM constructs along with the native linkers are outlined in Supporting Information: Figure S2. The SLIC primers used in this study are tabulated in Supporting Information: Table S1. The sequences for all CBM constructs generated are summarized in Supporting Information: Text S1. The CBM sequences used in this study correspond to the DNA fragments encoding CBM3a (amino acid residues 323–523 of the full-length CipA cellulosomal scaffoldin from *Clostridium thermocellum*; GenBank accession number CCV01464.1), CBM64 (amino acid residues 717–805 at the C-terminus of the full-length glycosyl hydrolase family 9 from *Spirochaeta thermophila*; GenBank accession number ADN02997.1), and CBM17 (amino acid residues 378–557 at the C-terminal substrate-binding domain CBM17 from *Clostridium cellulovorans* endo-1,4-beta glucanase EngF; GenBank accession number AAB40891.1). Briefly, the gene fragment containing the linker and CBM was amplified using polymerase chain reaction (PCR) from the original plasmid available at the Chundawat lab. It was inserted after the "GFP-CBM" region in the original "pEC-GFP-CBM" plasmids to create the "tandem CBM" (also referred to as "CBM-CBM") carrying plasmids. The insert and vector PCR products were purified to remove unreacted nucleotides (deoxynucleoside triphosphates or dNTPs), mixed at optimal ratios, and then transformed into chemically competent *E. cloni* 10G cells to get colonies for screening. The tandem plasmids developed were later used to create non-GFP versions by removing the GFP from those plasmids. All the pEC-GFP-CBM, pEC-GFP-CBM-CBM, and pEC-CBM-CBM plasmids were verified using Sanger sequencing, and the sequence-verified plasmids were stored at −80°C for long-term storage. *E. cloni* 10G cells carrying the plasmid of interest were stored as 15% glycerol stocks and maintained at −80°C.

2.3 | Production and purification of recombinant His-tagged CBMs

After sequence verification, all CBM constructs were transformed into *E. coli* BL21-CodonPlus-RIPL [λDE3]. Glycerol stocks were prepared for the transformed strains and were stored at −80°C. These glycerol stocks were later used to inoculate 10 mL Luria Bertani (LB) media in culture tubes containing kanamycin at a 50 μg/mL concentration. This overnight starter culture was used to inoculate 300 mL LB media in 1 L shake flasks containing kanamycin at a 50 μg/mL concentration. The flasks were incubated at 37°C and 200 rpm until the growth reached the exponential phase (OD_{600} ~0.6 to 0.8). Protein expression was then induced using 0.5 mM IPTG at 25°C for 16 h. Cells were harvested at 7000x*g* for 15 min. Three grams of cell pellet was resuspended in 15 mL cell lysis buffer (20 mM phosphate buffer, 500 mM NaCl, 20% [v/v] glycerol, pH 7.4). For every 3 g of wet cell pellet, 200 μL protease inhibitor cocktail (1 μM E-64 [Sigma Aldrich E3132]), and 15 μL lysozyme (Sigma Aldrich) was added. Cells were lysed on ice using a Misonix™ sonicator 3000 for 5 min of total process time at 4.5 output level and pulse settings (pulse-on time: 10 s and pulse-off time: 30 s) to avoid sample overheating. The cell lysate carrying the protein of interest was separated from the cell debris by centrifuging at 48,400x*g* for 45 min at 4°C. The cell lysate was clarified using a 0.22 μm non-sterile syringe filter after centrifugation. Since all the expressed CBMs contained an N-terminal 8X-HIS tag, the proteins were purified using IMAC (immobilized metal affinity chromatography). The clarified cell lysate was incubated with 2 ml pre-equilibrated Ni^{2+} charged magnetic resin purchased from GenScript. Briefly, the resin was equilibrated with five column volumes of buffer A (100 mM MOPS, 500 mM NaCl, 10 mM Imidazole, pH 7.4). The equilibrated resin was incubated with the clarified lysate at 4°C for 120 min with gentle agitation. The lysate was removed from the magnetic resin using a magnetic rack. The resin was later washed with five-column volumes of buffer A twice, followed by five-column volumes of (buffer A: buffer B = 95:5). Finally, the proteins were eluted out using five-column volumes of buffer B (100 mM MOPS, 500 mM NaCl, 500 mM Imidazole, pH 7.4). The purified proteins were later desalted into 10 mM MES buffer, pH 6.5 using PD-10 columns (GE HealthCare) according to the manufacturer's specifications. Proteins were also characterized for molecular weights and purity using SDS-PAGE (Supporting Information: Figure S3). The concentration of CBM proteins was estimated by measuring the absorbance at 280 nm. The molecular weight, extinction coefficient, and net charge (at pH 6.5) of all the CBM proteins used in this study are summarized in Supporting Information: Table S2. Proteins were later aliquoted, flash-frozen under liquid nitrogen, and stored at −80°C for further assays.

To confirm the presence of monomers/multimers in the purified & desalted proteins, single and tandem versions GFP-CBM3a and GFP-CBM64 were subjected to size exclusion chromatography (SEC). Briefly, 300 μL of purified protein (0.5 mg/mL) was applied to a Superdex 200 increase 10/300 GL HR column (Cytiva Life Sciences) equilibrated in 50 mM HEPES buffer, pH 6.5, at a flow rate of 1 mL/min.

10970290, 2023, 8, Downloaded from https://onlinelibrary.wiley.com/doi/10.1002/bit.28484 by National Renewable Energy Lab, Wiley Online Library on [03/08/2023]. See the Terms and Conditions (https://onlinelibrary.wiley.com/terms-and-conditions) on Wiley Online Library for rules of use; OA articles are governed by the applicable Creative Commons License

The distribution of monomers, dimers, and multimers were analyzed by measuring the UV absorbance at 280 nm and comparing their molecular weights to gel fitration standard (Bio–Rad 1511901). The percentage distribution of various oligomers was estimated using the area under the curve calculated using ChromLab software (Bio-Rad).

2.4 | Generation of PASC from Avicel cellulose-I

PASC was prepared according to the protocol detailed by Zhang et al. (2006). Briefly, 0.6 mL of distilled water was added to 0.2 g of Avicel cellulose-I (PH-101) to form a wet-cellulose slurry. To this slurry, 10 mL of 86.2% ice-cold phosphoric acid was added with vigorous stirring. The cellulose mixture turned transparent, after which 40 ml of ice-cold distilled water was added at a rate of 10 mL per min. The resulting white cloudy precipitate was removed by centrifugation at 5000x*g* for 20 min at 4°C. This step was repeated four more times to remove the phosphoric acid. In addition, 0.5 mL of 2 M sodium carbonate was added to neutralize the mixture. Finally, the mixture was washed in ice-cold DI water until the pH was between 5 and 7. The regenerated PASC was stored at 4°C for further binding assays.

2.5 | GFP-CBM pull-down binding assays with crystalline cellulose-I and PASC

Binding assays were performed as discussed in previous papers from our group (Chundawat et al., 2021; Nemmaru et al., 2021). Briefly, all binding assays were performed with at least six replicates in 300 µL 96-well round-bottomed polypropylene plates (USA Scientific). Each of these replicates was a 200 µL reaction mixture comprising appropriate volumes of CBM dilution to reach effective concentrations of 0–600 µg/mL for obtaining the full binding isotherm. In addition to the CBMs, the mixture comprised 2.5 mg of Avicel cellulose-I, an effective BSA concentration of 2.5 mg/mL to prevent nonspecific protein binding, and an effective buffer concentration of 10 mM MES (pH 6.5). To account for protein loss due to denaturation or nonspecific binding to the microwells, controls without cellulose were also included to obtain total protein concentration. The microplate was then sealed with a 96-well plate mat and incubated inside a USA Scientific hybridization oven at 5 rpm for 60 min at room temperature with end-over-end mixing. Never-shaken control reactions were also prepared, similar to shaken control reactions. This control was used to obtain the calibration curve relating GFP fluorescence and known protein concentration. After incubating the plate for an hour, the microplates were centrifuged at 2000 rpm for 2 min using an Eppendorf™ 5810 R centrifuge to separate cellulose from soluble supernatant. Finally, 100 µL of soluble supernatant was picked up from each microwell using a multichannel micropipette and transferred to black opaque microplates for measuring fluorescence at 480 nm excitation, 512 nm emission with 495 nm cut-off using Molecular Devices™ UV spectrophotometer. Schematic representation of the biochemical assay workflow is shown in Figure 1a.

2.6 | GFP-CBM pull-down binding assay data analysis

Preliminary data analysis was performed using Microsoft Excel™ to obtain free protein (µM) and bound protein concentrations (µmol/g cellulose). The data was fit to Langmuir one-site model using the nonlinear curve fitting tool in Origin for full-scale binding assays. Curve fitting was done using the Levenberg–Marquardt algorithm with a tolerance of 1e−9. Correlation analysis was performed using Pearson's correlation function available on Microsoft Excel™ to obtain the correlation coefficients between parameters and associated *p*-values to determine significance.

2.7 | Reversibility testing for single and tandem CBM constructs binding to cellulose substrates

A binding reversibility study was performed for all single and tandem CBMs after the completion of the original binding assays. After collecting the supernatant for measuring fluorescence in binding assays, 100 µL of reconstitution mixture (2.5 mg/mL BSA + 10 mM MES [pH 6.5]) was added to the remaining original reaction mixtures and shaken controls. The microplate was resealed with a 96-well plate mat and incubated at 5 rpm for 60 min at room temperature. After incubation, the supernatant was collected, and fluorescence was measured using the spectrophotometer, as mentioned above under the "pull-down binding assays" section.

2.8 | Preparation of nanocrystalline cellulose through acid hydrolysis for QCM-D analysis

Nanocrystalline cellulose was prepared from Avicel cellulose-I using the procedure mentioned previously (Nemmaru et al., 2021). Briefly, 2 g of Avicel cellulose-I was added to 70 mL 4 N hydrochloric acid (HCl) in a glass beaker placed over a water bath maintained at 80°C. The slurry was stirred every 30 min using a spatula to ensure uniform suspension. After 4 h, 50 mL of DI water was added to dilute the acid hydrolysis mixture. The slurry was split across 50 mL tubes and centrifuged at 1600x*g* for 10 min. The supernatant was discarded, and the pellet was resuspended in 10 mL DI water. This wash step was repeated multiple times until the solution turned hazy and the pH rose to around pH 3.3. The haziness of the supernatant indicated the development of cellulose nanocrystals, and these supernatants were collected for future usage.

2.9 | Preparation of cellulose thin films for QCM-D analysis

QCM-D sensors (4.95 MHz quartz crystals; Biolin Scientific QSX-301) were prepared in a manner as described previously (Nemmaru et al., 2021). Briefly, quartz crystals were washed thoroughly with deionized water, rinsed with ethanol, and dried with nitrogen gas.

10970290, 2023, 8, Downloaded from https://onlinelibrary.wiley.com/doi/10.1002/bit.28484 by National Renewable Energy Lab, Wiley Online Library on [03/08/2023]. See the Terms and Conditions (https://onlinelibrary.wiley.com/terms-and-conditions) on Wiley Online Library for rules of use; OA articles are governed by the applicable Creative Commons License

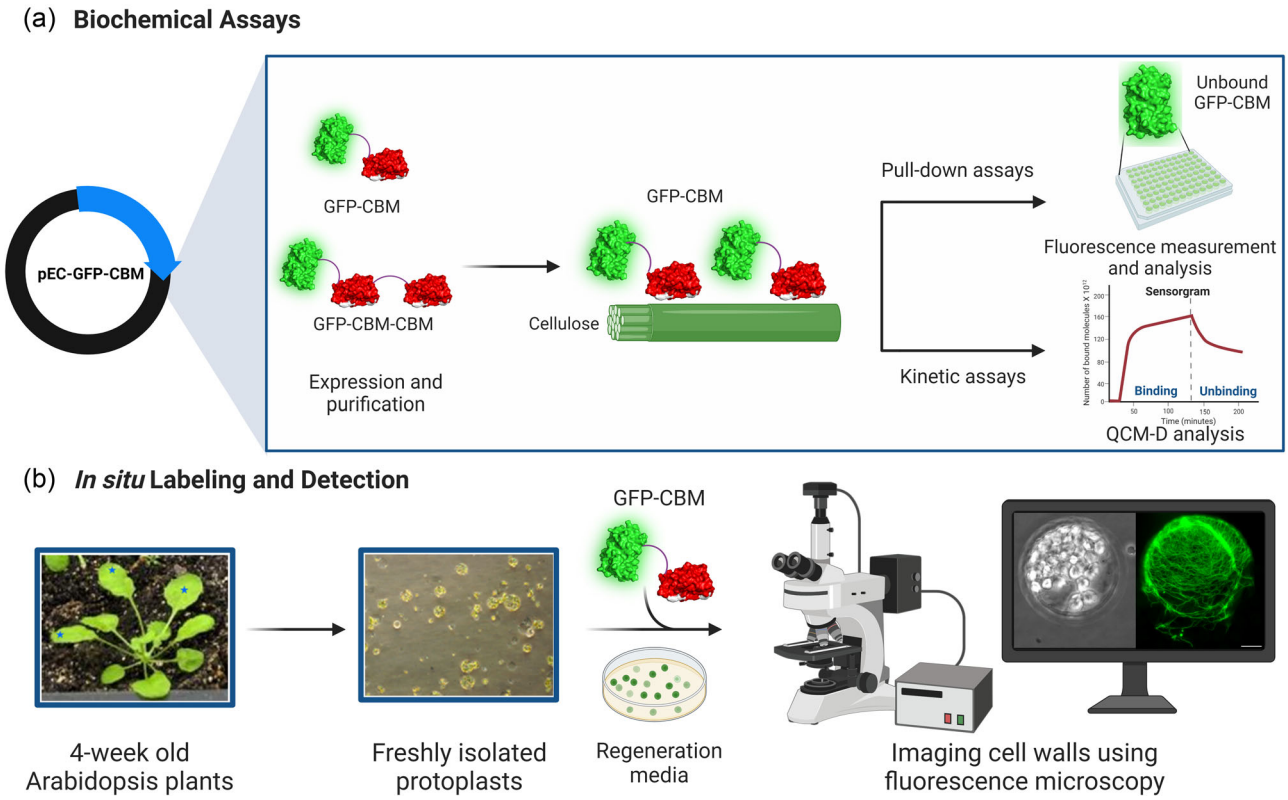

FIGURE 1 Schematic representation of the workflow in analyzing and utilizing GFP-CBMs to visualize regenerated plant cell walls. (a) pEC-GFP-CBM plasmid used for expressing GFP-CBM3a (*Clostridium thermocellum*) and GFP-CBM3a-CBM3a proteins. Purified proteins were used for estimating biochemical and kinetic cellulose binding parameters using pull-down assays and QCM-D analysis. (b) Medium-sized leaves from 4-week-old *Arabidopsis* plants (marked with blue stars) were used to isolate similarly sized protoplasts. Isolated protoplasts were incubated in the regeneration media along with GFP-CBMs. On the right, regenerated protoplasts with cell walls labeled with GFP-CBM3a as observed under fluorescence microscopy. CBM, carbohydrate-binding module; GFP, green fluorescent protein; QCM-D, quartz crystal microbalance with dissipation.

The sensors were then placed in a rack and submerged in a solution of 0.02% poly(diallyl dimethylammonium chloride), from Sigma Aldrich, for at least 60 min with orbital mixing (150 rpm) at room temperature. The sensors were then blown-dry once again, followed by spin-coating with 225 µL of cellulose nanocrystal slurry using a Chemat Technology KW-4A spin coater with a pre-cycle spin for 3 s at 1500 rpm, followed by a spin cycle for 60 s at 3000 rpm. This spin coating step is repeated four to eight times to obtain a uniform cellulose film thickness of ~20 to 40 nm (as measured using the QSoft software using the Sauerbrey model and an assumed density of 1191 kg/m^3). Note that the number of necessary cellulose spin coating steps is dependent on the concentration of cellulose nanocrystals in the prepared slurry and may need to be optimized on a case-to-case basis.

2.10 | QCM-D based CBM-cellulose kinetic binding assay

Binding and unbinding kinetic rate parameter estimation assays were performed on a QSense E4 instrument (Nanoscience Instruments). The quartz sensors with a deposited cellulose film were loaded into the instrument and allowed to equilibrate overnight in 10 mM MES buffer pH 6.5. Following the overnight incubation, the frequency and resonance changes associated with harmonics 1, 3, 5, 7, and 9 were tracked and monitored for stability for at least 5 min in the MES buffer before loading CBMs. All CBM proteins were diluted to a concentration of 5 µM and passed over the sensors at a flow rate of 100 µL/min for at least 10 min or until saturation was observed. Unbinding of proteins was tracked by flowing 10 mM MES buffer pH 6.5 at 100 µL/min for at least 20 min. The sensors and Qsense chambers were then rinsed with 5% Contrad solution followed by deionized water to remove any traces of residual protein. The frequency and dissipation traces were analyzed using an in-house data analysis routine based on binding and unbinding equations derived previously (Nemmaru et al., 2021).

2.11 | Analysis of QCM-D-based binding assay data to obtain kinetic parameters

Binding curves of QCM-D data were analyzed using RStudio based on equations derived previously (Nemmaru et al., 2021). Data

10970290, 2023, 8, Downloaded from https://onlinelibrary.wiley.com/doi/10.1002/bit.28484 by National Renewable Energy Lab, Wiley Online Library on [03/08/2023]. See the Terms and Conditions (https://onlinelibrary.wiley.com/terms-and-conditions) on Wiley Online Library for rules of use; OA articles are governed by the applicable Creative Commons License

corresponding to the frequency changes of the third harmonic of each experiment was transformed with the Sauerbrey equation to produce a change in mass (ng.cm^{-1}) associated with CBM binding and unbinding regime. The area of the sensor gaining mass was found to have a radius of 0.5 cm, and this value was used to determine the total ng of protein binding/unbinding to the cellulose surface.

It was noted that not all the mass that is added to the cellulose sensor is removed during the unbinding experiments, and that some CBM appears to remain bound even after extensive washing. We postulate that this may be due either to a difference in the nature and interaction of CBMs with the nanocellulose coating the surface compared to Avicel-based cellulosic materials in other pull-down experiments, or perhaps due to incomplete coating of the sensor surface with nanocellulose, allowing some CBM to bind irreversibly to the underlying poly(diallyl dimethylammonium chloride) layer. To accommodate this finding and provide a more suitable fit for the unbinding equation, the equation used to fit the unbinding data included a term (CBM_{remain}) which accounted for the irreversible CBM binding and represented the number of CBM molecules still bound to the sensor surface after washing. The inclusion of this term produced the following equation, which was used to fit the data.

$$[EC] = A \times \left(e^{-(k_{off} \times t)} + \frac{CBM_{remain}}{A}\right)$$

Where EC is the number of binding sites occupied by protein (μmol);

A is the number of available binding sites on nanocellulose film;

k_{off} is the dissociation rate constant (min^{-1});

t is the time (min);

CBM_{remain} is the number of CBM molecules that remain bound after washing.

The adsorption rate constant (nk_{on}) was calculated using the following equation:

$$nk_{on} = N_{max} x\ k_{off}(QCM\ kinetic\ binding\ assay) \\ x\ K_d(pull - down\ equilibrium\ binding\ assay)$$

Where nk_{on} is the adsorption rate constant (L.g^{-1}.min^{-1});

k_{off} is the desorption rate constant (min^{-1});

N_{max} is the maximum number of binding sites available on the substrate (μmol/g cellulose);

K_d is the binding dissociation constant (μM).

2.12 | Preparation of plant samples for imaging plant protoplasts

A. thaliana Col-0 (Columbia) was used as plant material for all experiments. *A. thaliana* mesophyll protoplasts were isolated as described in detail by Yoo et al. (2007). Briefly, 3 to 4-week-old, uniformly sized leaves were selected to obtain consistently sized protoplasts (Figure 1b). Thin leaf strips of 0.5–1 mm thickness were cut off from the middle portion of the leaves. These leaf strips were immediately transferred to an enzyme solution (0.4 M Mannitol, 20 mM KCl, 20 mM MES, 1.5% Cellulase R10 [Yakult], 0.4% Macerozyme R10 [Yakult], 10 mM $CaCl_2$, 5 mM 2-mercaptoethanol, 0.1% BSA). The leaf strips were vacuum infiltrated to perfuse it with the enzyme solution and then incubated in the dark for 3–5 h to digest the cell wall completely. The protoplasts were then diluted with an equal volume of sterile W5 solution (154 mM NaCl, 125 mM $CaCl_2$, 5 mM KCl, and 2 mM MES in ultrapure water). The undigested leaf material was filtered out using a pre-washed 75 μm nylon mesh. Protoplasts were then collected by centrifugation at 1000 rpm for 3 min at 4°C. The residual enzymatic solution was removed by washing the protoplast cells with 10 mL of W5 solution twice. After washing, the protoplasts were resuspended in 0.5 mL of W5 solution. The quality of the protoplasts was observed under a simple light microscope (Figure 1b). The concentration of protoplasts was measured using a hemocytometer and then adjusted to 2×10^5 protoplasts mL^{-1} of W5 solution. Next, 200 μL of protoplasts at 2×10^5 concentration was incubated in cell wall regeneration media containing an equal volume of WI solution (0.5 M Mannitol, 4 mM MES, 20 mM KCl) and 2M2 media (Gamborg's B-5 basal medium with minimal organics 6.4 g/L [Sigma], 0.8 M Trehalose, 0.1 M Glucose, 2 μM 3-naphthalene acetic acid [NAA] pH 5.7). The protoplasts were incubated for 17 h at room temperature under a Philips hue lamp. After incubation, the regenerated protoplasts were isolated by spinning at 300x*g* for 3 min at 4°C. The regenerated protoplasts were then fixed by incubation on ice for 10 min in 200 μL of 1% w/v glutaraldehyde. The protoplasts were then washed with 250 μL of 12% w/v sorbitol twice. Samples were resuspended in 50 μL of 12% w/v sorbitol and stored on ice until use.

2.13 | Fluorescence and CLSM

Calcofluor white solution (100 μL of 0.001%) was added to 200 μL of regenerated protoplasts and incubated at room temperature for 5 min. Excess calcofluor solution was removed after spinning down the cells at 1000 rpm for 2 min. The stained cells were washed with 12% sorbitol solution twice. Ten microliters of the regenerated protoplast samples were placed on a glass slide that was layered with a coverslip. Calcofluor-stained cell fibers were visualized under the DAPI channel in Olympus FSX 100 microscope. Staining using CBMs was done in a similar manner, where the final concentration of CBMs in the solution was 100 nM. Excess CBMs were removed, and the cells were observed under the GFP channel for GFP-CBMs and the red channel for DSR-CBMs.

For CLSM, the samples were prepared as mentioned above, and the glass slides were then placed onto the inverted platform of a Zeiss LSM 710 confocal microscope, and the cells were imaged under the 488 nm channel for GFP-CBMs and 561 nm channel for DSR-CBMs. All images were processed with Zeiss imaging software, ImageJ, or Adobe Photoshop.

10970290, 2023, 8, Downloaded from https://onlinelibrary.wiley.com/doi/10.1002/bit.28484 by National Renewable Energy Lab, Wiley Online Library on [03/08/2023]. See the Terms and Conditions (https://onlinelibrary.wiley.com/terms-and-conditions) on Wiley Online Library for rules of use; OA articles are governed by the applicable Creative Commons License

3 | RESULTS

3.1 | Tandem CBM3a shows reduced binding affinity compared to its single CBM counterpart

We prepared two type-A tandem CBMs, CBM3a (associated with the cellulosome-integrating protein A of *C. thermocellum*) (Lehtiö et al., 2003; Tormo et al., 1996; Yaniv et al., 2013), and CBM64 (associated with glycosyl hydrolases of *S. thermophila*) (Pires et al., 2017; Schiefner et al., 2016) by fusing the 42 amino acid native linker-CBM region to the N-terminal region of GFP-CBM as shown in Figure 2a. Additionally, we determined the equilibrium binding affinity of GFP-CBM and GFP-CBM-CBM tandem constructs toward Avicel cellulose-I and PASC, respectively (Figure 2b; Supporting Information: Figures S4–5).

First, we performed fluorescence-based pull-down binding assays for GFP-CBM3a and GFP-CBM64—single and tandem versions against Avicel cellulose-I at varying protein concentrations (ranging between 0 and 600 μg/mL). Nonspecific adsorption is avoided by adding BSA in the binding assays to block nonspecific binding sites on cellulose. Hence, we assume that the adsorption interactions observed arise largely from site specific binding. The resulting data were fitted to Langmuir isotherm one-site models to obtain the maximum number of binding sites (N_{max}) on the substrate, binding dissociation constant (K_d), and partition coefficient (see Table 1). Partition coefficient is slope of the initial linear region of the binding curve between bound protein (μmol/g cellulose) and free protein (μM). The number of available binding sites was the highest for GFP-CBM3a compared to other constructs. Regardless of the substrate (cellulose-I or PASC), GFP-CBM3a always showed a significant similarity in binding affinity (i.e., the inverse of K_d). The binding affinity was also observed to be higher for GFP-CBM3a compared to GFP-CBM3a-CBM3a against cellulose-I. Nevertheless, the binding affinity is comparable between the single and tandem versions of CBM64 toward cellulose-I although the number of binding sites is higher for GFP-CBM64-CBM64. GFP-CBM17 had the

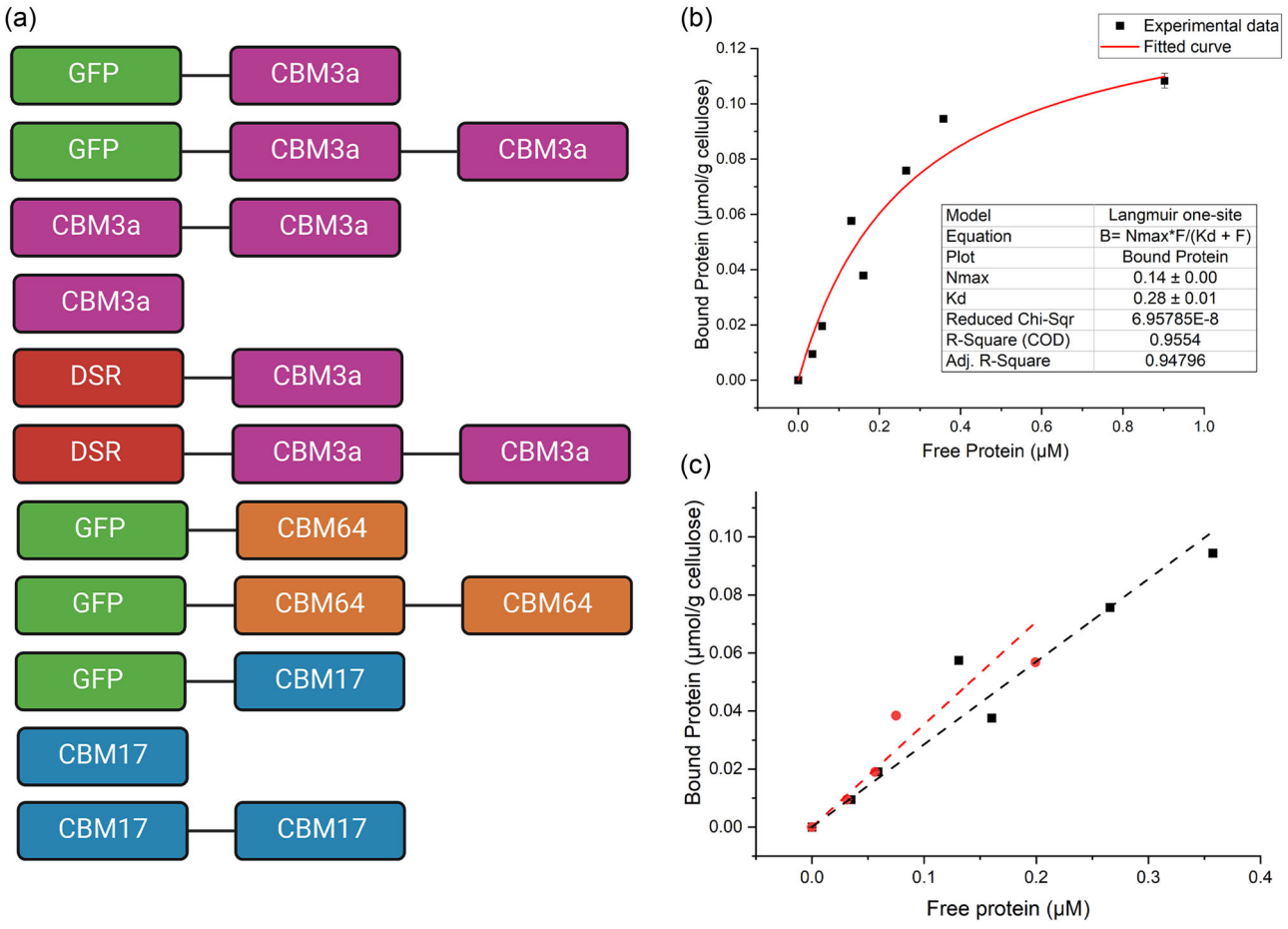

FIGURE 2 (a) Different protein construct designs tested in this study. (b) Equilibrium binding data (as black squares) of GFP-CBM3a toward cellulose-I fitted to a standard one-site Langmuir-type adsorption model (as red line). (c) Binding reversibility of GFP-CBM3a toward cellulose-I where black squares and red dots represent the original and re-equilibrated data points, respectively. Here, the red and black lines represents linear partition coefficient model fit for original and re-equilibrated data points, respectively. Representative full-scale binding curve and binding reversibility data is shown here for GFP-CBM3a but for all other binding curves and reversibility data set see Supporting Information: Figures S4-S7 in SI document. CBM, carbohydrate binding modules; GFP, green fluorescent protein.

10970290, 2023, 8, Downloaded from https://onlinelibrary.wiley.com/doi/10.1002/bit.28484 by National Renewable Energy Lab, Wiley Online Library on [03/08/2023]. See the Terms and Conditions (https://onlinelibrary.wiley.com/terms-and-conditions) on Wiley Online Library for rules of use; OA articles are governed by the applicable Creative Commons License

TABLE 1 Pull-down binding assay based parameters N_{max}, K_d, adjusted R^2, and reversibility for GFP-CBM3a, GFP-CBM3a-CBM3a, GFP-CBM64, GFP-CBM64-CBM64, and GFP-CBM17 obtained from Langmuir one-site model fitted to full-scale binding assay data.

Construct	N_{max} (μmol/g cellulose)	K_d (μM)	N_{max}/K_d (L/g cellulose)	Adjusted R^2	Reversibility
Cellulose-I					
GFP-CBM3a	143.27 ± 1.36	0.28 ± 0.01	0.51	0.95	+
GFP-CBM3a-CBM3a	87.99 ± 5.18	1.29 ± 0.26	0.07	0.99	+
GFP-CBM64	23.7 ± 1.11	0.29 ± 0.00	0.07	0.99	+
GFP-CBM64-CBM64	37.19 ± 3.14	0.30 ± 0.03	0.13	0.73	−
GFP-CBM17	93.82 ± 6.36	5.2 ± 0.35	1.71	0.99	−
PASC					
GFP-CBM3a	166.67 ± 0.91	0.30 ± 0.02	0.57	1	−
GFP-CBM3a-CBM3a	64.10 ± 0.54	0.29 ± 0.00	0.21	0.99	+
GFP-CBM64	130.24 ± 12.34	2.12 ± 0.00	0.06	0.99	+
GFP-CBM64-CBM64	113.81 ± 2.41	0.48 ± 0.00	0.23	1	+
GFP-CBM17	96.05 ± 26.51	0.93 ± 0.07	0.11	0.63	+

Note: Adjusted R^2 are obtained from the fitted Langmuir plots and reversibility data is obtained from reversibility studies as outlined elsewhere. Reversibility of CBMs is depicted as reversible (+) or irreversible (−). Errors are standard deviations of the mean obtained from the fitting analysis. Each experiment was performed using six replicates for each protein concentration.

Abbreviations: CBM, carbohydrate binding modules; GFP, green fluorescent protein; PASC, phosphoric acid swollen cellulose.

weakest affinity toward cellulose-I. The order of binding affinity observed toward cellulose-I is GFP-CBM3a ~ GFP-CBM64 ~ GFP-CBM64-CBM64 > GFP-CBM3a-CBM3a > GFP-CBM17.

Similarly, we subjected all the CBM constructs to binding assays against PASC. We observed a ~threefold reduction in N_{max} for the GFP tandem CBM3a compared to single CBM3a. The decrease in N_{max} for the tandem CBM3a could be due to the tendency of the tandem constructs to self-dimerize as indicated by size-exclusion chromatography. The binding affinity (i.e., inverse of K_d) was similar in case of both GFP-CBM3a and GFP-CBM3a-CBM3a. Similar to cellulose-I, there was no significant difference in the number of binding sites (N_{max}) available for GFP-CBM64, GFP-CBM64-CBM64, and GFP-CBM17. However, GFP-CBM64 had a reduced binding affinity compared to GFP-CBM64-CBM64 and other CBM constructs. The order of affinity toward PASC is GFP-CBM3a-CBM3a ~ GFP-CBM3a > GFP-CBM64-CBM64 > GFP-CBM17 > GFP-CBM64.

Furthermore, the partition coefficients of single CBM3a against cellulose-I and PASC were nearly seven- and twofold higher, respectively, than tandem CBM3a. This reduction in partition coefficient for tandem CBMs on PASC is probably due to the significant steric clashes it encounters on the surface of amorphous cellulose. The uneven topology of the hydrophobic binding face probably impairs the accessibility for tandem CBMs (Chundawat et al., 2021; Nemmaru et al., 2021). On the other hand, the GFP-CBM64 has a two- and a fourfold reduction in partition coefficient against cellulose-I and PASC, respectively, compared to tandem CBM64. GFP-CBM17 is highly specific to amorphous cellulose and therefore showed a significant reduction (~fivefold) in binding affinity and an increased partition coefficient toward cellulose-I versus PASC.

The reversibility of tandem CBMs has not been studied extensively in the reported literature, and often the reported binding reversibility data for single CBMs has been contradictory at times (Lim et al., 2014; Møller et al., 2021). It is imperative to study the binding reversibility since the application of Langmuir-type adsorption models is dependent on reversible binding of protein to substrate. The reversibility of binding of CBMs against cellulose-I and PASC was investigated in this study (Figure 2c; Supporting Information: Figures S6-S7). If the original binding data (black dashed line) and re-equilibrated data (red dashed line) coincided with each other, as indicated by overlapping Langmuir adsorption model fitted lines, CBM binding to cellulose is considered reversible (Supporting Information: Figures S6-7). To understand the extent of reversibility on a given substrate (i.e., cellulose I or PASC), we compared the initial binding slopes (i.e., partition coefficients at the initial stages of the binding curve) of the original and re-equilibrated data (see Supporting Information: Table S3 and S4 for Student's *t*-test results). A similar protocol was used in our previous studies (Lim et al., 2014; Nemmaru et al., 2021). Most of the CBM constructs were reversible on both the substrates ($p > 0.05$) although the extent of reversibility varied greatly (Table 1; Supporting Information: S3-4). We observed that the binding of single GFP-CBM3a is reversible on cellulose-I but almost irreversible on PASC ($p = 0.06$). However, tandem CBM3a is reversible on both cellulose-I and PASC, likely ruling out the possibility of protein denaturation or aggregation on the cellulose surface. GFP-CBM64 is found to be reversible on cellulose-I and PASC. Tandem

10970290, 2023, 8, Downloaded from https://onlinelibrary.wiley.com/doi/10.1002/bit.28484 by National Renewable Energy Lab, Wiley Online Library on [03/08/2023]. See the Terms and Conditions (https://onlinelibrary.wiley.com/terms-and-conditions) on Wiley Online Library for rules of use; OA articles are governed by the applicable Creative Commons License

CBM64 is slightly irreversible toward cellulose-I ($p = 0.08$) and not on PASC. Conversely, GFP-CBM17 is slightly irreversible on cellulose-I ($p = 0.07$) and reversible on PASC, as shown previously as well (Blake et al., 2006; Boraston et al., 2003). See Table 1, Supporting Information: Tables S3-S4 for a summary of binding reversibility, partition coefficients, and p-values of all the CBMs studied using cellulose-I and PASC.

3.2 | QCM-D assays reveal CBM-cellulose binding interactions to be protein design dependent

To characterize the binding kinetics of single and tandem CBMs on nanocrystalline cellulose, QCM-D binding assays were setup (Figure 3a). Briefly, the number of protein molecules bound to the cellulose film was calculated by converting the frequency data

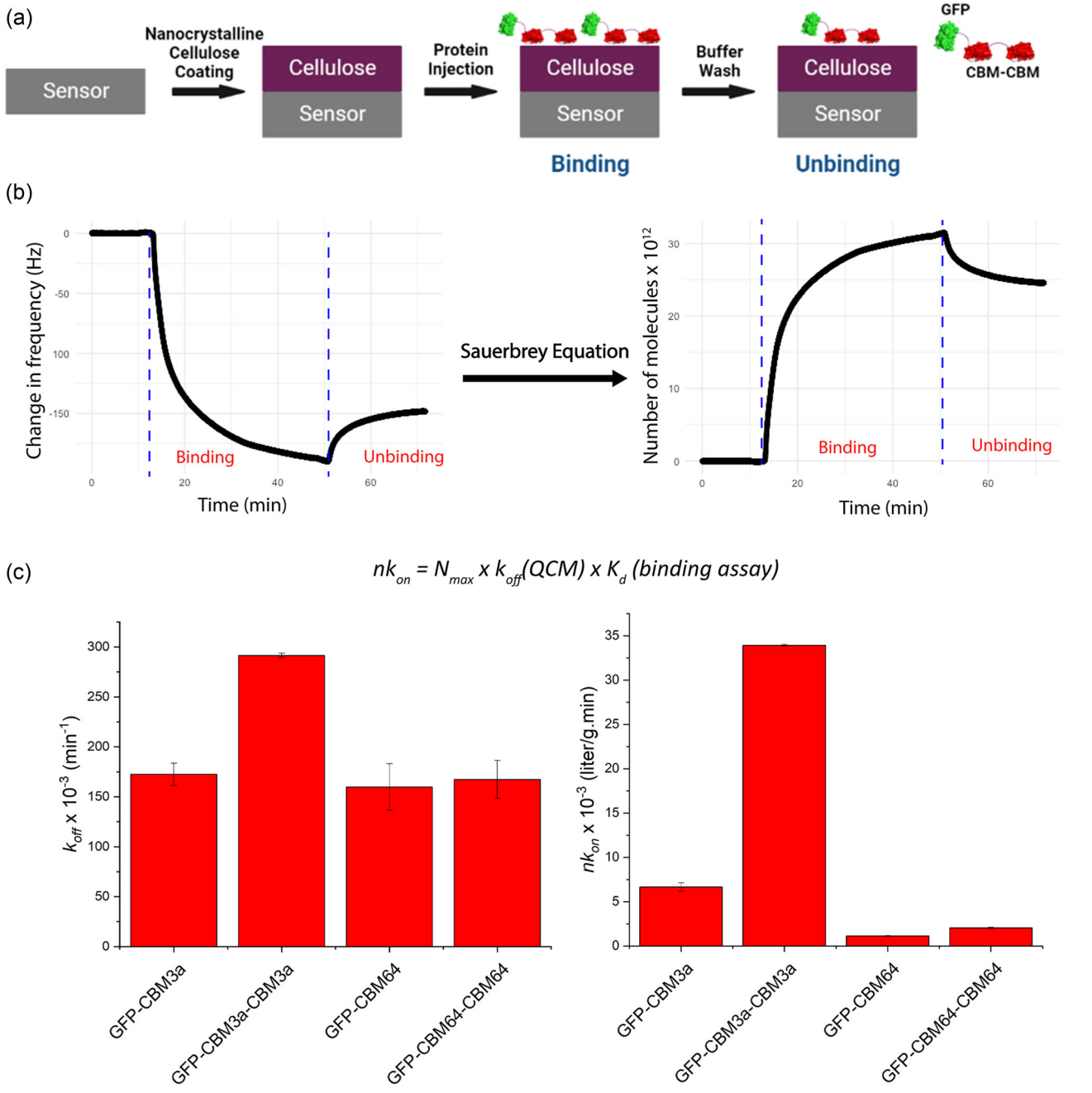

FIGURE 3 (a) Schematic representation for QCM-D-based tandem CBM—nanocrystalline cellulose-based binding assay setup. (b) Frequency (Hz) versus time (min) data for a representative protein (GFP-CBM3a) was converted to a sensorgram (number of protein molecules × 10^{12} vs. time [mins]) using the Sauerbrey equation. The binding and unbinding data in the plot on the right were then fitted to an exponential rise and decay function, respectively, as described in the methods section. (c) nk_{on} (right) was calculated using the formula stated here and k_{off} (left) was obtained from QCM-D analysis for GFP-CBM3a, GFP-CBM3a-CBM3a, GFP-CBM64, and GFP-CBM64-CBM64 toward cellulose-I. CBM, carbohydrate binding modules; GFP, green fluorescent protein.

10970290, 2023, 8, Downloaded from https://onlinelibrary.wiley.com/doi/10.1002/bit.28484 by National Renewable Energy Lab, Wiley Online Library on [03/08/2023]. See the Terms and Conditions (https://onlinelibrary.wiley.com/terms-and-conditions) on Wiley Online Library for rules of use; OA articles are governed by the applicable Creative Commons License

obtained from the binding and unbinding of proteins (Brunecky et al., 2020). Sauerbrey equation was used to obtain the mass of adsorbed protein on cellulose film using the frequency change (Kankare, 2002). In particular, the unbinding regime was fitted to an exponential decay to obtain the true desorption rate (k_{off}) as shown in Figure 3b. QCM-D raw data for all proteins along with their best fits are shown in Supporting Information: Figure S12. The effective adsorption rate constant (nk_{on}) was measured using desorption rate k_{off} from the QCM-D analysis and N_{max}, K_d obtained from the equilibrium pull-down binding assay results. These kinetic parameters were chosen since they were found to be an integral part of the kinetic models that were reported previously as well (Gao et al., 2013; Nemmaru et al., 2021). QCM-D analysis shows a ~1.7-fold increase in k_{off} for GFP-CBM3a-CBM3a compared to GFP-CBM3a, indicating a reduced binding affinity for tandem CBM3a compared to the single construct. However, the nk_{on} value for tandem CBM3a increased fivefold compared to the single CBM3a. Conversely, a similar trend was observed for the k_{off} values between tandem and single versions of CBM64 toward cellulose-I nanocrystals (Figure 3c). To account for any effects in k_{off} and nk_{on} values arising from GFP being fused with CBM3a, we also prepared tandem CBM3a and single CBM3a without GFP. Interestingly, the non-GFP version of CBM3a-CBM3a showed a reduction in the k_{off} value (nearly fivefold) compared to the GFP version (Supporting Information: Figure S8; Table 2), suggesting that GFP fusion may increase the off-rate for the tandem CBM3a. On the other hand, CBM3a seemed to have an increased off rate when GFP was removed. CBM17 protein constructs (GFP-CBM17, CBM17, and CBM17-CBM17) showed irreversible binding during the desorption phase in QCM-D experiments (data not shown), similar to the inconsistent pull-down binding assays observed against cellulose-I and were not used for further experiments/analysis. Hence, only type-A CBMs were chosen for cellulose visualization studies on regenerating protoplasts in this study. Also, GFP control showed very weak binding to nanocrystalline cellulose, and the number of bound molecules was found to be two orders of magnitude lower than values observed for all other tested CBMs (Supporting Information: Figure S12; Table 2).

In summary, GFP-CBM3a showed a reduced nk_{on} compared to GFP-CBM3a-CBM3a. Removing GFP reduced the off-rate drastically for tandem CBM3a but increased it for single CBM3a. On the other hand, CBM64 didn't have a significant difference in their k_{off} values. These results suggest that there is no significant difference in binding affinity for single and tandem versions of CBM64 toward cellulose-I. Also, a weaker binding is probably more prevalent in the case of GFP tandem CBM3a toward cellulose-I, which could be determined from a higher desorption rate which is overcome by removing GFP. The k_{off}, nk_{on}, and total number of bound molecules estimated from QCM-D assays are summarized in Table 2.

3.3 | Visualizing cellulose microfibrils after *A. thaliana* protoplast cell wall regeneration

Procedures for preparing *Arabidopsis* wild-type mesophyll protoplasts and cell wall regeneration conditions have been described in detail under the "Section 2." The isolated protoplasts were healthy and relatively homogeneous in size, as observed under a simple light microscope (Figure 1). After 17 h of incubation of protoplasts in regeneration media (WI + 2M2), the cells were fixed and stained with calcofluor, a β-glucan-specific dye (Supporting Information: Figure S9a). The regenerated cell wall network composed of mostly β-glucans like cellulose was spread over the entire surface of the plant protoplast. Similarly, GFP-CBM3a (100 nM) was used to visualize the regenerated cell wall under wide-field fluorescence microscopy. Both calcofluor and GFP-CBM3a stained cells showed the presence of fibrous structures on the surface of protoplasts after overnight incubation of protoplast cells in cell wall regeneration media. The developed fibers labeled by GFP-CBM3a were distinct and clear when observed under the green emission channel using a fluorescence microscope (Supporting Information: Figure S9b).

TABLE 2 Kinetic rate constants for GFP-CBM3a, GFP-CBM3a-CBM3a, GFP-CBM64, GFP-CBM64-CBM64, CBM3a, CBM-CBM3a, and GFP adsorption and desorption toward nanocrystalline cellulose allomorphs estimated using QCM-D-based binding assay data.

	k_{off} x 10^{-3} (min^{-1})	nk_{on} x 10^{-3} ($L.g^{-1}.min^{-1}$)	A (x10^{-12} bound molecules)
GFP-CBM3a	172.45 ± 11.11	6.65 ± 0.47	27.91 ± 2.26
GFP-CBM3a-CBM3a	291.56 ± 2.02	33.92 ± 0.00	18.20 ± 2.55
GFP-CBM64	159.86 ± 23.24	1.12 ± 0.00	17.89 ± 1.70
GFP-CBM64-CBM64	167.35 ± 19.02	2.03 ± 0.00	16.32 ± 0.00
CBM3a	223.12 ± 1.86	na	23.90 ± 0.42
CBM3a-CBM3a	64.24 ± 16.84	na	30.15 ± 0.70
GFP	181.42 ± 1.19	na	0.18 ± 0.00

Abbreviations: CBM, carbohydrate binding modules; GFP, green fluorescent protein; na, not available; QCM-D, quartz crystal microbalance with dissipation.

10970290, 2023, 8, Downloaded from https://onlinelibrary.wiley.com/doi/10.1002/bit.28484 by National Renewable Energy Lab, Wiley Online Library on [03/08/2023]. See the Terms and Conditions (https://onlinelibrary.wiley.com/terms-and-conditions) on Wiley Online Library for rules of use; OA articles are governed by the applicable Creative Commons License

3.4 | Type-A CBMs facilitate detailed visualization of protoplast cell walls by confocal microscopy

To explore further the general significance of the findings above, the other type-A CBMs analyzed biochemically were also used to image regenerated cell walls of plant protoplasts. All CBMs tested bound to the cell wall surface of protoplasts, as typical of type-A CBMs. CLSM was used to acquire images with high-resolution and across multiple focal planes. CLSM images showed that the regenerated plant protoplasts had a pronounced accumulation of fluorescence on the outer periphery of the protoplasts. Both GFP-CBM3a and GFP-CBM3a-CBM3a bound to fibrous stuctures on the cell wall compared to the control specimens with no added CBMs (Figure 4; Supporting Information: Videos 1-4). To check if other type-A tandem CBMs behave in a similar fashion, GFP-CBM64-CBM64 was used to also visualize the regenerated plant protoplasts. Cell wall fibers were observed throughout the outer periphery of the protoplasts in this case as well (Supporting Information: Figure S10; Videos 5). Alternatively, the DS-red versions of CBM3a also showed similar fibrous networks (Supporting Information: Figure S11; Videos 6-7). However, the autofluorescence arising from plant chloroplasts under the red channel could partly contribute to the signals arising from DS-red fluorescence (Krause & Weis, 1991). Hence, GFP tagged CBMs were used for further plant cell wall imaging experiments.

3.5 | GFP-CBM3a probe potentiates in situ imaging of cellulose synthesized by plant protoplasts

Previous studies on imaging of plant cell walls were performed using immunocytochemistry and indirect immunofluorescence (Knox, 2012; McCartney et al., 2006). In particular, the time course of imaging of plant cell walls was performed by isolating regenerated protoplasts at specific time intervals and labeling them with calcofluor (Kuki et al., 2017) or by directly visualizing plant roots using Pontamine Fast Scarlet 4B (S4B) dye (Anderson et al., 2010). Cases where specialized microfluidic chambers are built to trap protoplasts with continuous replenishment of media supplemented with CFW dye, poses a significant threat to the integrity of the protoplasts and fails to show individual cellulose fibers. These studies fail to capture the continuous dynamics of cellulose growth and subtle fiber movement on the surface of regenerating plant protoplasts. The absence of molecular probes that could be readily added to the regeneration media is one of the primary reasons for the lack of complete understanding of cellulose regeneration kinetics and other dynamic properties. Here, since type-A CBMs are specific to cellulose in plant cells it makes them attractive as in situ imaging probes to overcome the highlighted bottleneck.

To examine if CBMs are compatible with live protoplasts as in situ imaging probes and do not significantly interfere with the cell wall regeneration process, we added 100 nM of GFP-CBM3a to the

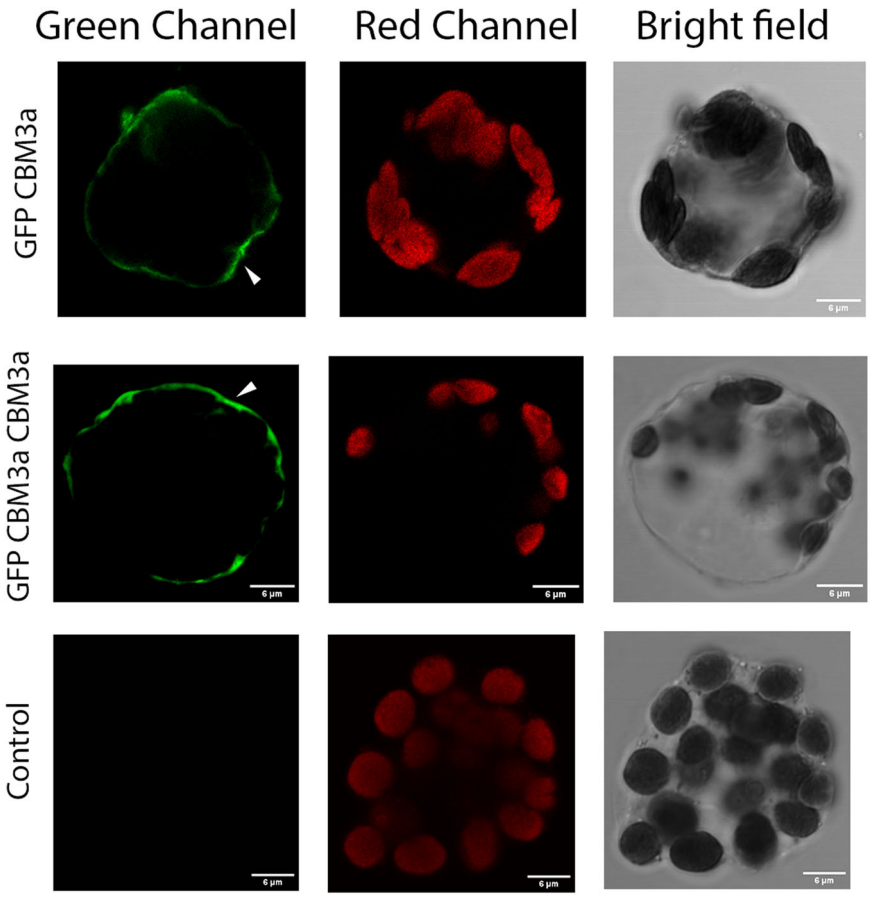

FIGURE 4 Confocal laser scanning microscopy images of GFP-CBM3a and GFP-CBM3a-CBM3a bound to regenerated plant cell walls of *Arabidopsis* mesophyll isolated single protoplast cells. The cell wall labeled with GFP-CBM is visible under the green channel (left), and chloroplasts are visible under the red channel due to autofluorescence (middle) and the bright field image showcases the overall intact protoplasts (right). Control had no GFP-CBM added before imaging. White arrows indicate the location of GFP-CBMs binding to peripheral regions of regenerated cell walls where cellulose deposition is expected to take place (scale bars, 6 µm). CBM, carbohydrate binding modules; GFP, green fluorescent protein.

10970290, 2023, 8, Downloaded from https://onlinelibrary.wiley.com/doi/10.1002/bit.28484 by National Renewable Energy Lab, Wiley Online Library on [03/08/2023]. See the Terms and Conditions (https://onlinelibrary.wiley.com/terms-and-conditions) on Wiley Online Library for rules of use; OA articles are governed by the applicable Creative Commons License

regeneration media (WI + M2) from the outset of the cell wall regeneration process. For controls, we had protoplasts in regeneration media with 100 nM GFP and no GFP or GFP-CBM3a. First, as mentioned previously, the regeneration of protoplasts was confirmed by adding GFP-CBM3a to the regenerated protoplasts. Cell wall fibers were clearly distinguishable and visible under fluorescence microscopy (Figure 5a). Similarly, protoplasts incubated in regeneration media, along with GFP-CBM3a, also exhibited a uniform distribution of cellulose at the cell surface compared to cells incubated with only GFP (Figure 5b). Taken together, these results show that GFP-CBMs could be potentially added to the protoplast cell wall regeneration media to continuously monitor the growing cellulose chains. Such a system should now provide researchers with the imaging tools needed to monitor cell wall growth and dynamics in real-time with live plant protoplast cells.

4 | DISCUSSION

Carbohydrate binding modules (CBMs) are crucial in targeting plant cell wall polysaccharides in coordination with specific glycosyl hydrolases (Fox et al., 2013; Hervé et al., 2010). Several studies show the presence of tandem CBMs coexisting with these modular microbial plant cell wall glycosyl hydrolases (Freelove et al., 2001; McCartney et al., 2006; Møller et al., 2021). Some of these tandem CBMs exhibit a synergistic effect with distinct specificities, and others exhibit an improved affinity toward polysaccharides. Unlike other plant polysaccharides that have an extensive repertoire of monoclonal antibodies (mAbs) readily available, no stable mAb exists that can be used to visualize cellulose (Rydahl et al., 2018). Calcofluor white has been traditionally used to obtain high-resolution fluorescent images of cellulose without autofluorescence (Kuki et al., 2017). Calcofluor is also known to bind to callose—a β−1,3 glucan present in plant cell walls. Besides nonspecific binding targets, calcofluor is also known to affect the in vivo assembly of cellulose microfibrils (Haigler et al., 1980). Hence, the presence of calcofluor in the cell wall regeneration media could potentially be toxic for plant cells and preclude its use in monitoring cell wall regeneration in live protoplasts. Some DNA aptamers have also been recently developed to visualize cellulose in plants (Głazowska & Mravec, 2021). However, proteinaceous probes offer a slight advantage since they could be readily engineered and reliably produced in diverse research labs. Type-A CBMs bind specifically to cellulose, and particularly, CBM3a has a high affinity toward cellulose making it an appropriate probe to detect plant cellulose (Chowdhury et al., 2014; Johnsen et al., 2015). However, CBM3a could also bind nonspecifically to other cell wall polysaccharides like xyloglucan (Hernandez-Gomez et al., 2015).

To improve the specificity, and predominantly visualize cellulose network around regenerated plant protoplasts, engineered CBMs could be ideal probes to be employed for imaging. To achieve this, we prepared tandem CBM3a fused to GFP to visualize cellulose formed in plant protoplasts directly. The ability of our tandem CBM3a design to recognize isolated cellulose both in vitro and in regenerated plant cell walls was assessed. It is important to note that it could be extremely challenging to isolate cellulose in its exact ultrastructure as present natively in plant cell walls. Hence, two different types of cellulose—highly crystalline (cellulose-I) and amorphous cellulose (PASC) were chosen as theoretical representatives of the two extreme types of ultrastructures of cellulose in plant cell walls. Interestingly, the tandem type-A CBMs—GFP-CBM3a and GFP-CBM64, showed reduced or equivalent binding affinity compared to their single domain counterparts. This reduction in binding affinity could be attributed to the presence of multimers as seen in the case of single GFP-CBMs for other type-A CBMs as well (Lim et al., 2014). To check if GFP-CBM3a and GFP-CBM64 form multimers in solution, we subjected both samples to SEC. Both the single CBMs showed high molecular weight multimeric aggregates and dimers (~15% and ~4%) compared to monomers (~82%). On the other hand, the tandem CBMs didn't show any large aggregates at all although they showed minimal amounts of dimers (4% and 9% corresponding to tandem CBM3a and tandem CBM64, respectively) and trimers (~2% to 3%) according to the predicted molecular weights (see Supporting Information: Figures S13-14 for SEC profiles, predicted molecular

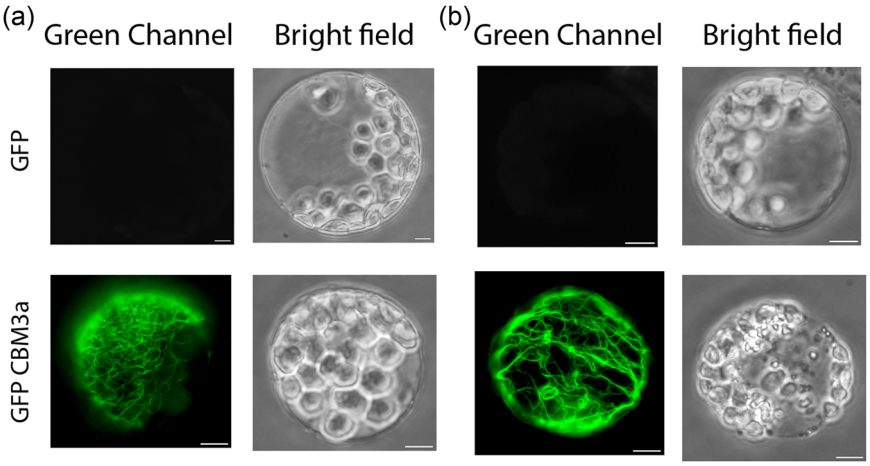

FIGURE 5 Fluorescence microscopy images of *Arabidopsis* plant protoplasts with regenerated cell walls. (a) GFP and GFP-CBM3a were added to the regenerated plant cell walls of *Arabidopsis* mesophyll protoplasts after 18 h incubation. (b) GFP and GFP-CBM3a were added along with the regeneration media at the outset of the 18 h incubation. Regenerated cellulose fibers labeled with GFP-CBM3a are visible under the green channel (left) and the bright field image of the intact protoplasts (right) (scale bars, 6 μm). CBM, carbohydrate binding modules; GFP, green fluorescent protein.

10970290, 2023, 8, Downloaded from https://onlinelibrary.wiley.com/doi/10.1002/bit.28484 by National Renewable Energy Lab, Wiley Online Library on [03/08/2023]. See the Terms and Conditions (https://onlinelibrary.wiley.com/terms-and-conditions) on Wiley Online Library for rules of use; OA articles are governed by the applicable Creative Commons License

weights, and percentage distribution of different oligomers seen for all constructs). The absence of large multimers could potentially explain the reduced binding affinity observed in case of GFP tandem CBM3a compared to single GFP-CBM3a. Also, the reduction in N_{max} values between single and tandem CBM3a in case of both cellulose-I and PASC could be due to the intramolecular protein–protein interactions in tandem CBM3a. These interactions in tandem CBMs along with the absence of multimers are speculated to explain some of the differences observed. In the case of CBM64, the affinity seems to be similar between single and tandem CBM64. The GFP tandem CBM64 is found to be both irreversible (Table 1) and the Langmuir model also doesn't seem to capture the exact fit (Adj. $R^2 = 0.73$). The relatively poor fit and the irreversibility of tandem CBM64 toward cellulose-I might be the reason behind the observed similar affinity to single GFP-CBM64 (Table 1). It is important to note that Langmuir model captures the saturation of binding as observed in our binding curves for most CBMs. However, this simple model has several drawbacks and it may not capture the exact binding behaviors for all proteins (e.g., poor fit is observed in the case of GFP-tandem CBM64 toward cellulose-I and GFP-CBM17 toward PASC). CBM17 is known to bind tightly toward PASC and was therefore used as a control in our study (Georgelis et al., 2012; Hackl et al., 2023). However, the poor fit (Adj. $R^2 = 0.63$) also elucidates that this model may not be best to explain different classes of CBMs. Therefore, the model seems to be dependent on the protein and substrate used. It is important to note that the model for other CBMs often showed a good fit (i.e., adj. R^2 is ~0.99–1). Moreover, while other models such as Langmuir two-site and Langmuir Freundlich have also been used for CBM binding assays, the simple one-site Langmuir adsorption models were found to be more appropriate than complex multisite adsorption models to estimate the minor differences in CBM binding affinity for distinct cellulosic allomorphs (Chundawat et al., 2021). Improved models are required in the future to get a better fit for some of the tested proteins. Further, studies involving the isolation of different multimers/oligomers corresponding to different peaks from size exclusion chromatograms and their corresponding binding affinities are required to address the observed phenomena in more detail.

The interaction between CBMs and its substrates has been shown to be affected by the net charge of the protein (Haarmeyer et al., 2017). Hence, the net charge and molecular weight (indicative of the tandem vs. single designs tested here) of a protein could also play a major role in explaining the binding differences observed for CBMs to cellulose. To identify any correlation between number of binding sites (N_{max}), binding dissociation constant (K_d) from pull-down binding assays with the standard protein structure parameters such as pI (isoelectric point), net charge, and molecular weight of the proteins, we ran a Pearson's correlation analysis between all available output/input parameters (pI, net charge, molecular weight, K_d, and N_{max}). The correlation coefficients along with their corresponding p-values are tabulated in Supporting Information: Tables S5-6. These correlation coefficient values range from +1 to −1. A value of +1 (green) means that the parameters are positively correlated and as one variable increases, so does the other. A value of −1 (red) means that the parameters are negatively correlated and as one variable increases, the other decreases and vice versa. A value of zero (white) means that there is simply no correlation seen. Net charge and pI of a protein seems to have a significant correlation ($p < 0.05$) with N_{max} of the proteins toward cellulose-I. Similarly, the net charge, pI, and molecular weight had the maximum correlation with K_d of the protein toward cellulose-I (Supporting Information: Table S5). Likewise, the correlation analysis for PASC revealed that the molecular weight of the protein had the most significant negative correlation ($p < 0.05$) with K_d and N_{max}, that is, as the molecular weight increases, the binding dissociation constant and the number of available binding sites decreases and vice versa (Supporting Information: Table S6).

QCM-D has been utilized as a tool to study the binding of full-length cellulases to different types of cellulose (Brunecky et al., 2020), lignin, and pretreated biomass (Haarmeyer et al., 2017; Kumagai et al., 2014). QCM-D has also been used to study CBMs associated with oxidases (Mollerup et al., 2016) and cellulase–hemicellulase complexes (Freelove et al., 2001). These reports were mostly confined to single wild-type and engineered CBMs associated with cellulases and other hydrolytic enzymes. We have previously examined the viscoelastic properties of CBM-cellulose binding using QCM-D analysis (Chundawat et al., 2021; Nemmaru et al., 2021). Here, we explored the kinetic constants of tandem CBMs using QCM-D to identify if they have an improved binding affinity and if they could be used as a weak or tight-binding cellulose imaging probes for plant cell walls. A similar trend in adsorption and desorption rate constants was observed in CBM64 for both tandem and single versions suggesting no apparent binding avidity advantage for tandem CBM64. Similar behavior was observed in SusF, a starch-utilizing system with tandem CBMs which didn't show an improved affinity compared to its single and mutated versions (Cameron et al., 2012). In contrast, GFP tandem CBM3a showed a higher adsorption and desorption rate under QCM-D analysis compared to GFP-CBM3a. Also, the reduction in number of bound molecules in the case of GFP tandem CBM3a compared to single GFP-CBM3a, suggests possible intramolecular CBM3a–CBM3a interactions in the protein as well as steric hindrance that the protein undergoes upon binding on the nanocrystalline cellulose surface. Interestingly, removing GFP seemed to decrease off-rate for tandem CBM3a drastically, suggesting that it might be more suitable probe for indirect immunofluorescence imaging purposes that involve a continuous and dynamic movement of the substrate in an aqueous environment. Additionally, these non-GFP-CBM versions could be conjugated to various amine-reactive fluorophores providing a library of CBMs that are compatible for live cell imaging across different imaging wavelengths. The resulting fluorophore conjugated CBM proteins may exhibit greater photostability and brighter fluorescence than other fluorochromes (Moran-Mirabal et al., 2009). To further understand any correlation between desorption rate (k_{off}) and the number of bound molecules (A) from QCM analysis with the protein parameters such as net charge, molecular weight, and pI, we also ran Pearson's correlation analysis between all the parameters

10970290, 2023, 8, Downloaded from https://onlinelibrary.wiley.com/doi/10.1002/bit.28484 by National Renewable Energy Lab, Wiley Online Library on [03/08/2023]. See the Terms and Conditions (https://onlinelibrary.wiley.com/terms-and-conditions) on Wiley Online Library for rules of use; OA articles are governed by the applicable Creative Commons License

(pI, net charge, molecular weight, k_{off}, and A) as outlined earlier. Here, pI and net charge seemed to have a positive significant correlation with the number of bound molecules ($p < 0.05$). The desorption rate seems to be dependent on pI the most (Supporting Information: Table S7).

Multimerization, net charge, molecular weight (indicative of tandem vs. single design), and linker length between proteins could all play a critical role in binding irreversibly to cellulose fibers. The native linker used in this study is 42 amino acids long and has been found to be highly flexible in our previous study (Bandi et al., 2020). Compared to shorter linker lengths, the inclusion of a flexible linker resulted in a reduced activity when fused to a cellulase CD (CelE from *C. thermocellum*). Similar behavior was observed when double CBMs were fused to cellulases, Cel6A and Cel7A (from *Trichoderma reesei*) during which a 48 aa-linker decreased the binding affinity and capacity of the tandem CBM compared to reduced linker lengths (Arola & Linder, 2016). However, a detailed study might be required to better understand the effect of linker length and binding affinity/reversibility of CBMs toward distinct cellulosic substrates.

In summary, these results provide diverse qualitative and quantitative facets of the single and tandem CBMs used for imaging cellulose fibers. Although single CBMs show a reduced desorption rate from QCM-D assays, confocal imaging of plant protoplasts shows distinct cell walls with both single and tandem-CBMs. However, GFP-CBM3a tends to bind irreversibly to PASC (which resembles the amorphous nature of cellulose) according to our study. Likewise, GFP-CBM64-CBM64 and GFP-CBM17 were observed to bind irreversibly to cellulose-I. Such irreversible binding probes might form aggregates on the regenerating cell surface and potentially impact cell wall regeneration when incubated in the regeneration media. However, the tandem CBM3a seems to be reversible on both cellulose-I and PASC. Such a reversible binding probe circumvents the aggregate issues (as observed under size-exclusion chromatography) and has a reduced desorption rate and an increased adsorption rate (as observed under QCM analysis) when the GFP is removed. Since the cellulose ultrastructure present in plant cell wall during the early stages of cell development is speculated to be largely amorphous, we recommend tandem CBM3a as a potential probe for all live plant cell imaging experiments for study of plant polysaccharides biosynthesis and cell wall regeneration. Furthermore, the plant cell wall is a natural amalgam of multiple polysaccharides intertwined with each other. Mimicking the exact composition of complex plant cell wall polysaccharides and the ultrastructure of cellulose in vitro might be unfeasible. To overcome the nonspecific binding nature exhibited by CBMs, techniques like phage display and directed evolution might be needed to engineer proteinaceous probes with greater specificity and affinity for imaging cellulose or other glycans synthesized and assembled in plant cell walls (DeVree et al., 2021). Lastly, an important characteristic of the GFP-CBM approach for detection and monitoring of cellulose fibers in plant cells is its relative compatibility with the regeneration medium. Long-term stability and compatibility property of GFP-CBMs opens up the possibility for direct visualization of the kinetic and spatial properties during the process of cell wall synthesis by using similar protein-based probes for visualizing cellulose.

AUTHOR CONTRIBUTIONS

Dharanidaran Jayachandran and Shishir P. S. Chundawat designed the research. Dharanidaran Jayachandran, Peter Smith, Mohammad Irfan, and Junhong Sun conducted research. Dharanidaran Jayachandran and Peter Smith analyzed the data. Dharanidaran Jayachandran and Shishir P. S. Chundawat wrote the manuscript with input from all authors.

ACKNOWLEDGMENTS

The authors acknowledge primary funding support from the US Department of Energy (Award Number: DE-SC0019313) and Rutgers University (Office of the Vice Chancellor for Research & Innovation). Funding for portion of the work was also provided by the Center for Bioenergy Innovation (CBI), a US Department of Energy Bioenergy Research Center supported by the Office of Biological and Environmental Research in the DOE Office of Science.

CONFLICT OF INTEREST STATEMENT

The authors declare no conflict of interest.

DATA AVAILABILITY STATEMENT

All raw data used to support the findings of this study are available upon request from the corresponding author (Shishir Chundawat; shishir.chundawat@rutgers.edu).

ORCID

Dharanidaran Jayachandran http://orcid.org/0000-0002-8672-2631
Peter Smith http://orcid.org/0000-0002-9276-5099
Mohammad Irfan http://orcid.org/0000-0002-7877-5530
Yannick J. Bomble http://orcid.org/0000-0001-7624-8000
Eric Lam http://orcid.org/0000-0001-8462-9794
Shishir P. S. Chundawat http://orcid.org/0000-0003-3677-6735

REFERENCES

Anderson, C. T., Carroll, A., Akhmetova, L., & Somerville, C. (2010). Real-time imaging of cellulose reorientation during cell wall expansion in *Arabidopsis* roots. *Plant Physiology*, *152*, 787–796.

Arola, S., & Linder, M. B. (2016). Binding of cellulose binding modules reveal differences between cellulose substrates. *Scientific Reports*, *6*, 35358.

Bandi, C. K., Goncalves, A., Pingali, S. V., & Chundawat, S. P. S. (2020). Carbohydrate-binding domains facilitate efficient oligosaccharides synthesis by enhancing mutant catalytic domain transglycosylation activity. *Biotechnology and Bioengineering*, *117*, 2944–2956.

Beckham, G. T., Ståhlberg, J., Knott, B. C., Himmel, M. E., Crowley, M. F., Sandgren, M., Sørlie, M., & Payne, C. M. (2014). Towards a molecular-level theory of carbohydrate processivity in glycoside hydrolases. *Current Opinion in Biotechnology*, *27*, 96–106.

Blake, A. W., McCartney, L., Flint, J. E., Bolam, D. N., Boraston, A. B., Gilbert, H. J., & Knox, J. P. (2006). Understanding the biological rationale for the diversity of cellulose-directed carbohydrate-binding modules in prokaryotic enzymes. *Journal of Biological Chemistry*, *281*, 29321–29329. https://doi.org/10.1074/jbc.M605903200

10970290, 2023, 8, Downloaded from https://onlinelibrary.wiley.com/doi/10.1002/bit.28484 by National Renewable Energy Lab, Wiley Online Library on [03/08/2023]. See the Terms and Conditions (https://onlinelibrary.wiley.com/terms-and-conditions) on Wiley Online Library for rules of use; OA articles are governed by the applicable Creative Commons License

Boraston, A. B., Bolam, D. N., Gilbert, H. J., & Davies, G. J. (2004). Carbohydrate-binding modules: Fine-tuning polysaccharide recognition. *Biochemical Journal*, *382*, 769–781.

Boraston, A. B., Kwan, E., Chiu, P., Warren, R. A. J., & Kilburn, D. G. (2003). Recognition and hydrolysis of noncrystalline cellulose. *Journal of Biological Chemistry*, *278*, 6120–6127. https://doi.org/10.1074/jbc.M209554200

Brady, S. K., Sreelatha, S., Feng, Y., Chundawat, S. P. S., & Lang, M. J. (2015). Cellobiohydrolase 1 from *Trichoderma reesei* degrades cellulose in single cellobiose steps. *Nature Communications*, *6*, 10149.

Brunecky, R., Subramanian, V., Yarbrough, J. M., Donohoe, B. S., Vinzant, T. B., Vanderwall, T. A., Knott, B. C., Chaudhari, Y. B., Bomble, Y. J., Himmel, M. E., & Decker, S. R. (2020). Synthetic fungal multifunctional cellulases for enhanced biomass conversion. *Green Chemistry*, *22*, 478–489.

Cameron, E. A., Maynard, M. A., Smith, C. J., Smith, T. J., Koropatkin, N. M., & Martens, E. C. (2012). Multidomain carbohydrate-binding proteins involved in *Bacteroides thetaiotaomicron* starch metabolism. *Journal of Biological Chemistry*, *287*, 34614–34625.

Chowdhury, J., Henderson, M., Schweizer, P., Burton, R. A., Fincher, G. B., & Little, A. (2014). Differential accumulation of callose, arabinoxylan and cellulose in nonpenetrated versus penetrated papillae on leaves of barley infected with *Blumeria graminis* f. sp. hordei. *New Phytologist*, *204*, 650–660.

Chundawat, S. P. S., Nemmaru, B., Hackl, M., Brady, S. K., Hilton, M. A., Johnson, M. M., Chang, S., Lang, M. J., Huh, H., Lee, S. H., Yarbrough, J. M., López, C. A., & Gnanakaran, S. (2021). Molecular origins of reduced activity and binding commitment of processive cellulases and associated carbohydrate-binding proteins to cellulose III. *Journal of Biological Chemistry*, *296*, 100431. https://doi.org/10.1016/j.jbc.2021.100431

DeVree, B. T., Steiner, L. M., Głazowska, S., Ruhnow, F., Herburger, K., Persson, S., & Mravec, J. (2021). Current and future advances in fluorescence-based visualization of plant cell wall components and cell wall biosynthetic machineries. *Biotechnology for Biofuels*, *14*, 78. https://doi.org/10.1186/s13068-021-01922-0

Drula, E., Garron, M. L., Dogan, S., Lombard, V., Henrissat, B., & Terrapon, N. (2022). The carbohydrate-active enzyme database: Functions and literature. *Nucleic Acids Research*, *50*, D571–D577.

Fox, J. M., Jess, P., Jambusaria, R. B., Moo, G. M., Liphardt, J., Clark, D. S., & Blanch, H. W. (2013). A single-molecule analysis reveals morphological targets for cellulase synergy. *Nature Chemical Biology*, *9*, 356–361.

Freelove, A. C. J., Bolam, D. N., White, P., Hazlewood, G. P., & Gilbert, H. J. (2001). A novel carbohydrate-binding protein is a component of the plant cell wall-degrading complex of *Piromyces equi*. *Journal of Biological Chemistry*, *276*, 43010–43017. https://doi.org/10.1074/jbc.M107143200

Gao, D., Chundawat, S. P. S., Sethi, A., Balan, V., Gnanakaran, S., & Dale, B. E. (2013). Increased enzyme binding to substrate is not necessary for more efficient cellulose hydrolysis. *Proceedings of the National Academy of Sciences*, *110*, 10922–10927.

Georgelis, N., Yennawar, N. H., & Cosgrove, D. J. (2012). Structural basis for entropy-driven cellulose binding by a type-A cellulose-binding module (CBM) and bacterial expansin. *Proceedings of the National Academy of Sciences*, *109*, 14830–14835.

Guillén, D., Sánchez, S., & Rodríguez-Sanoja, R. (2010). Carbohydrate-binding domains: Multiplicity of biological roles. *Applied Microbiology and Biotechnology*, *85*, 1241–1249.

Głazowska, S., & Mravec, J. (2021). An aptamer highly specific to cellulose enables the analysis of the association of cellulose with matrix cell wall polymers in vitro and in muro. *The Plant Journal*, *108*, 579–599.

Haarmeyer, C. N., Smith, M. D., Chundawat, S. P. S., Sammond, D., & Whitehead, T. A. (2017). Insights into cellulase-lignin non-specific binding revealed by computational redesign of the surface of green fluorescent protein. *Biotechnology and Bioengineering*, *114*, 740–750.

Hackl, M., Power, Z., & Chundawat, S. P. S. (2023). Oriented display of cello-oligosaccharides for pull-down binding assays to distinguish binding preferences of glycan binding Proteins. *bioRxiv*, 2023.01.26.525732. https://doi.org/10.1101/2023.01.26.525732

Haigler, C. H., Brown, R. M., & Benziman, M. (1980). Calcofluor white ST alters the in vivo assembly of cellulose microfibrils. *Science*, *210*, 903–906.

Hashimoto, H. (2006). Recent structural studies of carbohydrate-binding modules. *Cellular and Molecular Life Sciences*, *63*, 2954–2967.

Hernandez-Gomez, M. C., Rydahl, M. G., Rogowski, A., Morland, C., Cartmell, A., Crouch, L., Labourel, A., Fontes, C. M. G. A., Willats, W. G. T., Gilbert, H. J., & Knox, J. P. (2015). Recognition of xyloglucan by the crystalline cellulose-binding site of a family 3a carbohydrate-binding module. *FEBS Letters*, *589*, 2297–2303.

Hervé, C., Rogowski, A., Blake, A. W., Marcus, S. E., Gilbert, H. J., & Knox, J. P. (2010). Carbohydrate-binding modules promote the enzymatic deconstruction of intact plant cell walls by targeting and proximity effects. *Proceedings of the National Academy of Sciences*, *107*, 15293–15298.

Johnsen, H. R., Striberny, B., Olsen, S., Vidal-Melgosa, S., Fangel, J. U., Willats, W. G. T., Rose, J. K. C., & Krause, K. (2015). Cell wall composition profiling of parasitic giant dodder (*Cuscuta reflexa*) and its hosts: A priori differences and induced changes. *New Phytologist*, *207*, 805–816.

Kankare, J. (2002). Sauerbrey equation of quartz crystal microbalance in liquid medium. *Langmuir*, *18*, 7092–7094.

Kellett, L. E., Poole, D. M., Ferreira, L. M., Durrant, A. J., Hazlewood, G. P., & Gilbert, H. J. (1990). Xylanase B and an arabinofuranosidase from *Pseudomonas fluorescens* subsp. cellulosa contain identical cellulose-binding domains and are encoded by adjacent genes. *Biochemical Journal*, *272*, 369–376.

Knox, J. (2008). Revealing the structural and functional diversity of plant cell walls. *Current Opinion in Plant Biology*, *11*, 308–313.

Knox, J. P. (2012). In situ detection of cellulose with carbohydrate-binding modules, *Methods in enzymology* (Vol. 510, 1st ed., pp. 233–245). Elsevier Inc. https://doi.org/10.1016/B978-0-12-415931-0.00012-4

Kognole, A. A., & Payne, C. M. (2018). Cellulose-specific Type B carbohydrate binding modules: Understanding oligomeric and non-crystalline substrate recognition mechanisms. *Biotechnology for Biofuels*, *11*, 319. https://doi.org/10.1186/s13068-018-1321-7

Krause, G. H., & Weis, E. (1991). Chlorophyll fluorescence and photosynthesis: The basics. *Annual Review of Plant Physiology and Plant Molecular Biology*, *42*, 313–349.

Kuki, H., Higaki, T., Yokoyama, R., Kuroha, T., Shinohara, N., Hasezawa, S., & Nishitani, K. (2017). Quantitative confocal imaging method for analyzing cellulose dynamics during cell wall regeneration in *Arabidopsis* mesophyll protoplasts. *Plant Direct*, *1*, e00021.

Kumagai, A., Iwamoto, S., Lee, S. H., & Endo, T. (2014). Quartz crystal microbalance with dissipation monitoring of the enzymatic hydrolysis of steam-treated lignocellulosic nanofibrils. *Cellulose*, *21*, 2433–2444.

Lehtiö, J., Sugiyama, J., Gustavsson, M., Fransson, L., Linder, M., & Teeri, T. T. (2003). The binding specificity and affinity determinants of family 1 and family 3 cellulose binding modules. *Proceedings of the National Academy of Sciences*, *100*, 484–489.

Levine, S. E., Fox, J. M., Blanch, H. W., & Clark, D. S. (2010). A mechanistic model of the enzymatic hydrolysis of cellulose. *Biotechnology and Bioengineering*, *107*, 37–51.

Lim, S., Chundawat, S. P. S., & Fox, B. G. (2014). Expression, purification and characterization of a functional carbohydrate-binding module from *Streptomyces* sp. SirexAA-E. *Protein Expression and Purification*, *98*, 1–9. https://doi.org/10.1016/j.pep.2014.02.013

10970290, 2023, 8, Downloaded from https://onlinelibrary.wiley.com/doi/10.1002/bit.28484 by National Renewable Energy Lab, Wiley Online Library on [03/08/2023]. See the Terms and Conditions (https://onlinelibrary.wiley.com/terms-and-conditions) on Wiley Online Library for rules of use; OA articles are governed by the applicable Creative Commons License

McCartney, L., Blake, A. W., Flint, J., Bolam, D. N., Boraston, A. B., Gilbert, H. J., & Knox, J. P. (2006). Differential recognition of plant cell walls by microbial xylan-specific carbohydrate-binding modules. *Proceedings of the National Academy of Sciences*, *103*, 4765–4770.

McKie, V. A., Vincken, J. P., Voragen, A. G. J., Van Den Broek, L. A. M., Stimson, E., & Gilbert, H. J. (2001). A new family of rhamnogalacturonan lyases contains an enzyme that binds to cellulose. *Biochemical Journal*, *355*, 167–177.

Mollerup, F., Parikka, K., Vuong, T. V., Tenkanen, M., & Master, E. (2016). Influence of a family 29 carbohydrate binding module on the activity of galactose oxidase from *Fusarium graminearum*. *Biochimica et Biophysica Acta (BBA)-General Subjects*, *1860*, 354–362. https://doi.org/10.1016/j.bbagen.2015.10.023

Moran-Mirabal, J. M., Corgie, S. C., Bolewski, J. C., Smith, H. M., Cipriany, B. R., Craighead, H. G., & Walker, L. P. (2009). Labeling and purification of cellulose-binding proteins for high resolution fluorescence applications. *Analytical Chemistry*, *81*, 7981–7987.

Møller, M. S., El Bouaballati, S., Henrissat, B., & Svensson, B. (2021). Functional diversity of three tandem C-terminal carbohydrate-binding modules of a β-mannanase. *Journal of Biological Chemistry*, *296*, 100638.

Nemmaru, B., Ramirez, N., Farino, C. J., Yarbrough, J. M., Kravchenko, N., & Chundawat, S. P. S. (2021). Reduced type-A carbohydrate-binding module interactions to cellulose I leads to improved endocellulase activity. *Biotechnology and Bioengineering*, *118*, 1141–1151.

Zhang, Y.-H. P., Cui, J, Lynd, L. R., & Kuang, L. R. (2006). A transition from cellulose swelling to cellulose dissolution by o-phosphoric acid: Evidence from enzymatic hydrolysis and supramolecular structure. Biomacromolecules, *7*, 644–648.

Pires, V. M. R., Pereira, P. M. M., Brás, J. L. A., Correia, M., Cardoso, V., Bule, P., Alves, V. D., Najmudin, S., Venditto, I., Ferreira, L. M. A., Romão, M. J., Carvalho, A. L., Fontes, C. M. G. A., & Prazeres, D. M. (2017). Stability and ligand promiscuity of type A carbohydrate-binding modules are illustrated by the structure of *Spirochaeta thermophila* StCBM64C. *Journal of Biological Chemistry*, *292*, 4847–4860.

Ruel, K., Nishiyama, Y., & Joseleau, J. P. (2012). Crystalline and amorphous cellulose in the secondary walls of *Arabidopsis*. *Plant Science*, *193–194*, 48–61. https://doi.org/10.1016/j.plantsci.2012.05.008

Rydahl, M. G., Hansen, A. R., Kračun, S. K., & Mravec, J. (2018). Report on the current inventory of the toolbox for plant cell wall analysis: Proteinaceous and small molecular probes. *Frontiers in Plant Science*, *9*, 1–20.

Schiefner, A., Angelov, A., Liebl, W., & Skerra, A. (2016). Structural basis for cellulose binding by the type A carbohydrate-binding module 64 of *Spirochaeta thermophila*. *Proteins: Structure, Function, and Bioinformatics*, *84*, 855–858.

Shang, B. Z., Chang, R., & Chu, J. W. (2013). Systems-level modeling with molecular resolution elucidates the rate-limiting mechanisms of cellulose decomposition by cellobiohydrolases. *Journal of Biological Chemistry*, *288*, 29081–29089.

Stevenson, J., Krycer, J. R., Phan, L., & Brown, A. J. (2013). A practical comparison of ligation-independent cloning techniques. *PLoS One*, *8*, e83888.

Talamantes, D., Biabini, N., Dang, H., Abdoun, K., & Berlemont, R. (2016). Natural diversity of cellulases, xylanases, and chitinases in bacteria. *Biotechnology for Biofuels*, *9*, 133.

Tormo, J., Lamed, R., Chirino, A. J., Morag, E., Bayer, E. A., Shoham, Y., & Steitz, T. A. (1996). Crystal structure of a bacterial family-III cellulose-binding domain: A general mechanism for attachment to cellulose. *The EMBO Journal*, *15*, 5739–5751.

Vermaas, J. V., Kont, R., Beckham, G. T., Crowley, M. F., Gudmundsson, M., Sandgren, M., Ståhlberg, J., Väljamäe, P., & Knott, B. C. (2019). The dissociation mechanism of processive cellulases. *Proceedings of the National Academy of Sciences*, *116*, 23061–23067.

Whitehead, T. A., Bandi, C. K., Berger, M., Park, J., & Chundawat, S. P. S. (2017). Negatively supercharging cellulases render them lignin-resistant. *ACS Sustainable Chemistry & Engineering*, *5*, 6247–6252.

Xu, Y., Li, R., Luo, H., Wang, Z., Li, M. W., Lam, H. M., & Huang, C. (2022). Protoplasts: Small cells with big roles in plant biology. *Trends in Plant Science*, *27*, 828–829. https://doi.org/10.1016/j.tplants.2022.03.010

Yaniv, O., Morag, E., Borovok, I., Bayer, E. A., Lamed, R., Frolow, F., & Shimon, L. J. W. (2013). Structure of a family 3a carbohydrate-binding module from the cellulosomal scaffoldin CipA of *Clostridium thermocellum* with flanking linkers: Implications for cellulosome structure. *Acta crystallographica. Section F, Structural biology and crystallization communications*, *69*, 733–737.

Yoo, S. D., Cho, Y. H., & Sheen, J. (2007). Arabidopsis mesophyll protoplasts: A versatile cell system for transient gene expression analysis. *Nature Protocols*, *2*, 1565–1572.

SUPPORTING INFORMATION

Additional supporting information can be found online in the Supporting Information section at the end of this article.

How to cite this article: Jayachandran, D., Smith, P., Irfan, M., Sun, J., Yarborough, J. M., Bomble, Y. J., Lam, E., & Chundawat, S. P. S. (2023). Engineering and characterization of carbohydrate-binding modules for imaging cellulose fibrils biosynthesis in plant protoplasts. *Biotechnology and Bioengineering*, *120*, 2253–2268. https://doi.org/10.1002/bit.28484

10970290, 2023, 8, Downloaded from https://onlinelibrary.wiley.com/doi/10.1002/bit.28484 by National Renewable Energy Lab, Wiley Online Library on [03/08/2023]. See the Terms and Conditions (https://onlinelibrary.wiley.com/terms-and-conditions) on Wiley Online Library for rules of use; OA articles are governed by the applicable Creative Commons License